International Journal of Machine Tools & Manufacture 154 (2020) 103568

Contents lists available at ScienceDirect

International Journal of Machine Tools and Manufacture

journal homepage: http://www.elsevier.com/locate/ijmactool

A novel self-centring drill bit design for low-trauma bone drilling

Liming Shu [a,*], Shihao Li [a], Makoto Terashima [b], Wei Bai [c], Takayoshi Hanami [b], Ryo Hasegawa [b], Naohiko Sugita [a]

[a] Department of Mechanical Engineering, School of Engineering, The University of Tokyo, 7-3-1 Hongo, Bunkyo-ku, Tokyo, 113-8656, Japan
[b] TOKO Co., ltd, 5-27-10, Hongo, Bunkyo-ku, Tokyo, 113-0033, Japan
[c] State Key Lab of Digital Manufacturing Equipment and Technology, Huazhong University of Science and Technology, Wuhan, 430074, China

ARTICLE INFO

Keywords:
Bone
Drill bit
Damage reduction
Temperature
Force
Drill skidding

ABSTRACT

Drilling is one of the most common procedures in orthopaedic surgery. However, drilling-induced trauma occurs frequently and affects the processing damage and position accuracy of the holes, which strongly influence the postoperative recovery. Therefore, there is an urgent need to design a dedicated drill bit that can satisfy low-trauma requirements such as low cutting force, low temperature, self-centring, and low surface damage during orthopaedic surgery. In this work, a novel three-step drill structure is proposed to modify the cutting conditions at the entrance and exit of drilling, to effectively reduce the mechanical and thermal damages and improve the position accuracy in bone drilling. As the first step drill, a unique tip with thinned web was adopted by considering the drill skidding mechanisms under a non-perpendicular drilling condition. The second step was achieved by using an optimal point angle for balancing the effects of the cutting force and temperature. Moreover, a transition arc design was proposed as the third step to adjust the point angle during the finishing stage for switching the cutting mechanism from 'fracture & shear crack' cutting to 'shear' cutting in association with a certain range of feeding rates. This could reduce the mechanical and thermal damages to the finished hole surface. Drilling experiments under various process conditions demonstrated that the proposed drill design significantly reduced the drilling force, temperature, and damage and also improved the position accuracy of the holes compared to the conventional drill design. The proposed design provides an effective tool to achieve low-trauma bone drilling in orthopaedic surgery.

1. Introduction

Bone drilling is an indispensable and technically demanding procedure required for numerous orthopaedic surgeries, such as fracture fixation, joint replacement, and dental implantation. The desired outcome of the bone drilling process is the machining of accurately positioned and clean holes without trauma to the surrounding tissue. However, research on bone drilling is challenging owing to the complex material properties and operating conditions. The cortical bone, which is the main material that is processed during bone surgery, is a semi-brittle material with high strength, anisotropic characteristics, and low thermal conductivity. Fracture in the cortical bone is dependent not only on the magnitude of the applied stress, but also on the nature of intrinsic or induced cracks, which is a characteristic of the semi-brittle material [1]. Large-scale fractures can occur easily during bone resection, resulting in poor surface quality and damage to the surrounding tissues. In addition, the complex thermo-mechanical state and fracture during bone drilling may cause irreversible destruction of the tissues as well as peripheral blood vessels and nerves, which reduces the quality of surgery and affects postoperative recovery.

Recent reviews have concluded that the main challenges in bone drilling are tool breakage, heat development, drill skidding, and mechanical damage [2–5]. First, heat development during bone drilling can induce thermal necrosis, which might lead to bone necrosis, implant instability [6], and damage to the surrounding nerves [7]. It is generally accepted that the temperature threshold until which there are no changes in bone tissue morphology is 47 °C for 30 s [8]. Second, large cutting forces and torques may result in drill bit breakage [9], which would obstruct the placement of other devices and cause adverse histological effects. Third, to achieve the surgical goals, surgeons may need to drill at non-perpendicular orientations and on highly irregular bone surfaces without any fixtures. Because the working length of a drill bit in

* Corresponding author.
E-mail address: l.shu@mfg.t.u-tokyo.ac.jp (L. Shu).

https://doi.org/10.1016/j.ijmachtools.2020.103568
Received 31 January 2020; Received in revised form 27 April 2020; Accepted 27 April 2020
Available online 30 April 2020

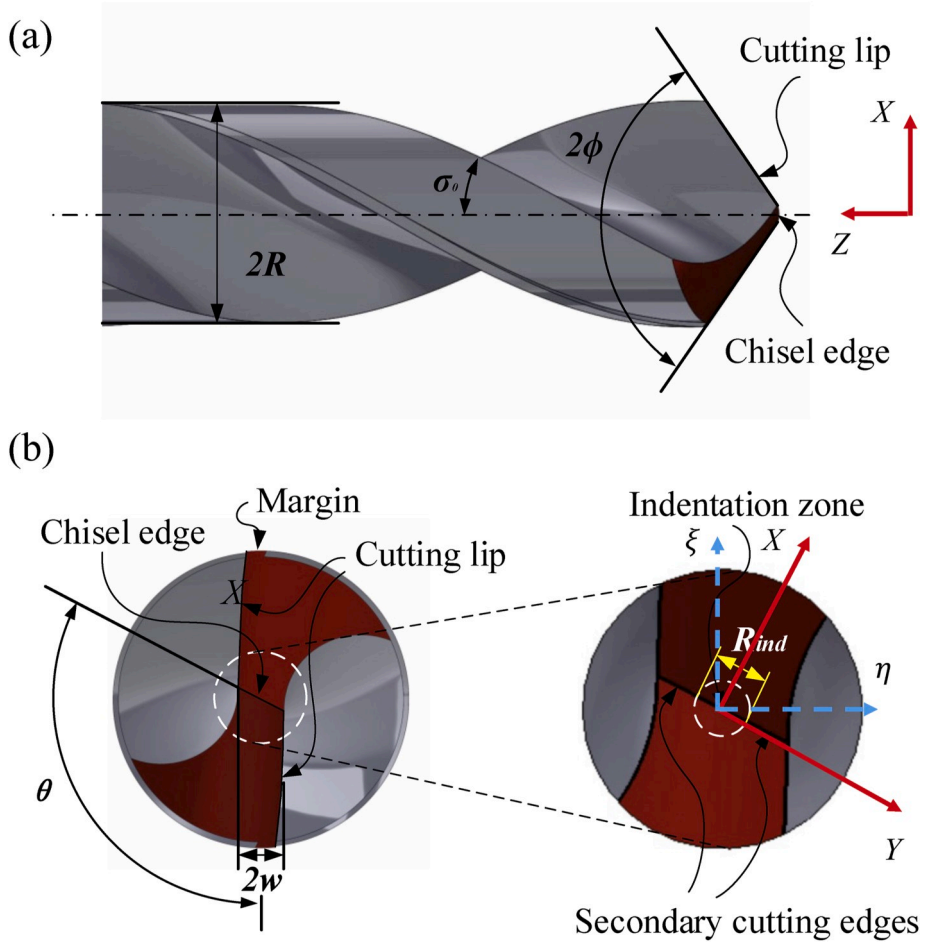

Fig. 1. Conical point twist drill bit geometry (a) and the three main cutting regions (b) (The basically geometry parameters are point angle (2φ), helix angle (σ_0), drill diameter ($2R$), web thickness ($2w$), and angle of the chisel edge (θ)).

orthopaedic surgery is typically longer than 60 mm and the diameter is smaller than 4.2 mm, this frequently causes skidding of the drill tip along the bone surface. This can result in damage to the surrounding soft tissue, tool breakage, and inaccurate positioning of the drill hole, which affect the requirements of position accuracy during implant assembly [10]. Fourth, the cortical bone is a semi-brittle material that exhibits biological activity, so that fracture is easy to generate and propagate inside the bone tissue. Micro-cracks can easily occur in drilling, which will decrease the screw pull-out strength and have an adverse effect on fracture healing [11]. Therefore, the development of a low-trauma surgical drill bit having low cutting force, low temperature rise, self-centring capability, and low surface damage is necessary.

Most of the drill bits widely used in surgeries have concepts and geometries similar to those developed for metal cutting. For example, the step drill bit, which was designed for the drilling of metals and composite materials for sufficiently reducing the cutting force and improving the surface quality [12], was introduced in the medical field. However, it was found that it increases the volume of the drilled bone, operation time, temperature elevation, and duration of bone drilling [2, 13]. Augustin et al. [14] concluded that the step drill has no significant advantage with regard to the temperature elevation in comparison with a standard twist drill of the same diameter. Thus, it is typically difficult to solve the main challenges in conventional bone drilling owing to the relatively complex material properties of bones and operation conditions of drilling. In the past ten years, the fundamental principles of bone cutting have been widely investigated by numerous researchers for improving the tool performance. Sugita et al. [15,16] presented the variation of chip morphologies of bone with the cutting depth and directions in orthogonal cutting operations. Fracture cutting can be observed when the cutting depth exceeds 80 μm [15,16]. He et al. [17] investigated the bone chip formation mechanisms in craniotomy and found that the microstructure and sub-microstructure of the cortical bone plays a great role in chip formation. Recently, Liao and Axinte [18] contributed considerably to understanding different cutting mechanisms for explaining the cutting performances for various cutting depths (d_{cut}). In addition, it was found that the average temperature elevation and cutting force were significantly reduced with increasing rack angle and cutting depth, changing the cutting model from shear cutting (10 μm < d_{cut}) to fracture cutting (d_{cut} > 90 μm) [19].

Several novel bone cutting methods and tools have been proposed based on different bone cutting mechanisms. Sugita et al. [20] developed a multi-grooved milling tool to reduce the cutting force and temperature during bone resection based on the fracture characteristics of bones. Liao et al. [21] further proposed a milling cutter with a main cutting edge and micro-cutting edges arranged on an Archimedes spiral for combining fracture cutting with shear cutting, which significantly reduced the surface damage and cutting temperature of the bone. Shu et al. [22,23] presented an elliptical vibration sawing device for reducing the surface damage, cutting force, and temperature based on fracture analysis of the bone and elliptical vibration cutting mechanics. Although many scholars have provided different solutions to the challenges of bone drilling by changing the processing parameters, there are few studies on the design of orthopaedic drill bits. Sui et al. [24], and Lee et al. [25], developed a mechanistic model of bone drilling to understand the effects of the design and processing parameters of a conventional drill bit on the cutting force. Bertollo et al. [10,26] conducted

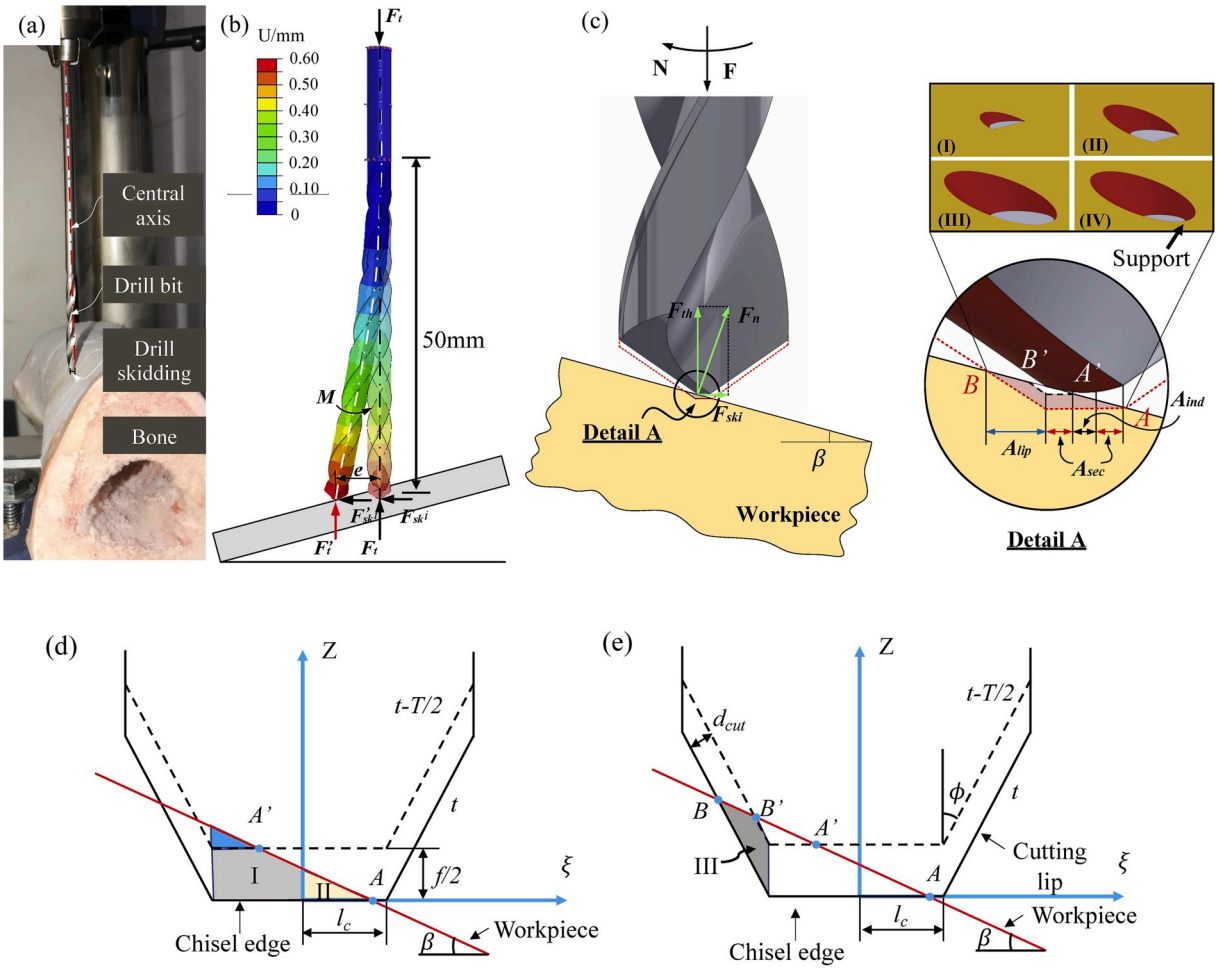

Fig. 2. (a) Skidding phenomena during in-vitro orthopaedic bone drilling, (b) schematic of drill bit bending during non-perpendicular drilling (finite element analysis of a 3.2 mm drill bit with the skidding force in the X direction ($F_{ski\text{-}X} = 5$ N)), (c) schematic of dynamic cutting during non-perpendicular drilling, (d) chisel edge cutting during non-perpendicular drilling, (e) cutting-lip cutting during non-perpendicular drilling. (A_{ind}, A_{sec}, and A_{lip} are the chip area of indentation zone, secondary cutting edge, and cutting lips, respectively. Zone I and II are the dynamic chip areas related to the chisel edge, which are divided by the z-axis plane, and Zone III is the dynamic unequal chip area in the cutting lips.)

several studies to prevent drill skidding in bone drilling, and concluded that a three-fluted orthopaedic drill has a high banding stiffness and screw pull-out strength. Zhang et al. [27] investigated five kinds of commercial drill bits through in-vivo histological studies and found that the drill bit geometry, including flute number and chisel edge, has a strong effect on bone damage. Feldmann et al. [28] proposed a custom-manufactured single-flute drill bit with a high rake angle and small chisel edge for reducing the temperature elevation in bone drilling. However, to the best of our knowledge, there is still no research that considers all the main challenges in the design of orthopaedic drill bits: self-centring capability, low cutting force, low temperature rise, and reduced surface damage.

In this study, the primary objective is to develop a low-trauma drill design for improving the position accuracy and reducing the mechanical and thermal damage based on the change in the cutting conditions at the entrance and exit of drilling with a specific geometrical design of the drill bit. First, a comprehensive theoretical analysis of the drill skidding, thermo-mechanistic, and material failure mechanisms in the orthopaedic drilling of a bone was conducted. Subsequently, a novel three-step drill bit design concept that satisfies the requirements of low trauma and self-centring was identified for application in orthopaedic surgery. Finally, comprehensive experimental tests were conducted in a state-of-the-art microscopy infrared thermography and dynamometer coupled bone cutting system to demonstrate the performance of the novel design in comparison with the conventional surgical drill bit.

2. Improvement of the orthopaedic drill bit

The most conventional and widely used orthopaedic drill is the conical point twist drill bit, as shown in Fig. 1. Two coordinate systems, the inertial system (XYZ) and the drill body rotation system ($\zeta\eta z$), were established for developing a unified treatment of dynamic drilling. The drill body rotation system ($\zeta\eta z$) is a system attached to the drill bit. As shown in Fig. 1(b), the directions of the ζ and η axes are defined parallel and perpendicular to the top view of the cutting lip. The z direction is defined consistent with the drill axis. The X, Y, and Z directions of the inertial system are consistent with the coordinate system of a dynamometer. The two coordinate systems are consistent when the drill bit first contacts the bone surface.

2.1. Drill skidding mechanism analysis

Fig. 2(a and b) present the skidding phenomena during non-perpendicular drilling. Drills become bent by skidding much easily

than their conventional counterparts in large-aspect-ratio holes, which are highly needed in orthopaedic drilling. The drill skidding mechanism during non-perpendicular drilling should be considered under two scenarios where the slope angle (β) are larger and smaller than $90-\varphi$, respectively. For $0<\beta<90-\varphi$, the cutting stage is illustrated in Fig. 2 (c). The cutting lip and unilateral secondary cutting edge are initially in contact with the bone surface. A skidding force (F_{ski}) is generated owing to the asymmetry of the cutting area on both sides of the X-plane, as displayed in stage I. Subsequently, F_{ski} is increased with the indentation zone and the entire secondary cutting-edge penetrating the bone surface, as shown in stages II and III. Drill skidding tends to be prohibited as a support bone (stage IV) emerges on the lower side of the hole with the increase in cutting depth. F_{ski} maintains a dynamic balance with the force generated by the elastic bending deformation of the drill bit. In addition, it is known that the cutting action of the chisel edge bears most of the thrust force during bone drilling [24]. Thus, the improvement of the chisel edge is critical for preventing drill skidding. When $\beta \geq 90-\varphi$, only the cutting lips and the margin will contact the bone surface. This makes drilling difficult because there is no positioning centre and a large skidding force is produced under this condition. In practice, a surgeon will initially drill a shallow hole in the perpendicular direction and then gradually adjust the direction of the drill to achieve the target orientation of the hole. Thus, in practice, it can be assumed that during drilling, the slope angle is smaller than β. Therefore, the drill skidding mechanism in $0<\beta<90-\varphi$ was mainly analysed.

For non-perpendicular drilling on a surface with a slope angle (Fig. 2 (d)), the position of the workpiece in the drill body rotation system can be determined by a coordinate system transformation as follows:

$$z_w = -(\xi\cos\omega t - \eta\sin\omega t)\tan\beta + l_c\tan\beta + \frac{f\omega t}{2\pi} \tag{1}$$

where ω is the rotation speed in rad/s, t is the cutting time, f is the feeding speed in mm/rev, l_c is the half length of the chisel edge, and $l_c = -w/\tan\theta$.

In addition, the coordinate of the chisel edge can also be expressed based on the definition of the drill body rotation system as

$$\begin{cases} \eta = -\xi\tan\theta \\ z = 0 \end{cases} \tag{2}$$

where θ is the chisel edge angle.

The intersection point of the chisel edge (A) on the workpiece can be obtained by combining Eqs. (1) and (2), as

$$\xi_A = \frac{f\omega t + 2\pi l_c\tan\beta}{2\pi(\cos\omega t + \tan\theta\sin\omega t)\tan\beta} \tag{3}$$

The increase in F_{ski} in the chisel edge is a result of the unequal chip area. Thus, the locations of the intersection points of the chisel edge (A') in the previous cut on the workpiece (Fig. 2 (d)) should be calculated as

$$\xi_{A'} = \frac{-2\pi l_c\tan\beta - f\omega\left(t-\frac{T}{2}\right)}{2\pi(\cos\omega t + \tan\theta\sin\omega t)\tan\beta} \tag{4}$$

where T is the rotation period of the drilling. Therefore, the dynamic unequal chip area produces F_{ski} in the chisel edge, which is divided into two unequal parts by the z-axis plane, as follows:

$$\Delta A_c = A_I - A_{II} = \frac{fl_c - \left(\xi_A^2 + \xi_{A'}^2\right)\tan\beta}{2} \tag{5}$$

The maximum chip area difference (ΔA_{c-max}) as the entire chisel edge penetrates the workpiece can be calculated as

$$\Delta A_{c-max} = \frac{l_c^2\tan\beta}{2} \tag{6}$$

The intersection point of the cutting lip (B) on the workpiece can be calculated by combining the coordinates of the cutting lip and workpiece in the $\zeta\eta z$ system, as shown in Fig. 2 (e), as

$$\xi_B = \frac{2\pi l_c(\cot\varphi + \tan\beta) + f\omega t + 2\pi w\sin\omega t\tan\beta}{2\pi(\cot\varphi + \cos\omega t\tan\beta)} \tag{7}$$

The location of the intersection point (B') of the cutting lip in the previous cut on the workpiece is

$$\xi_{B'} = \frac{2\pi l_c(\cot\varphi + \tan\beta) + f\omega\left(t-\frac{T}{2}\right) - 2\pi w\sin\omega t\tan\beta}{2\pi(\cot\varphi - \cos\omega t\tan\beta)} \tag{8}$$

Thus, the dynamic unequal chip area related to the cutting lips can be expressed as

$$\Delta A_l = A_{III} = \left[(\xi_A + l_c)(\xi_B - l_c)\tan\beta - (\xi_{B'} - l_c)\left((\xi_A + l_c)\tan\beta - \frac{f}{2}\right)\right] \Big/ 2 \tag{9}$$

The maximum unequal chip area from the cutting lip when the entire chisel edge penetrates the workpiece can be obtained by geometrical analysis as

$$\Delta A_{l-max} = \frac{2l_c^2\tan\beta}{\tan\varphi - \tan\beta} - \left(\frac{2l_c\tan\beta}{\tan\varphi - \tan\beta} - \frac{f\cos\beta}{2\sin(\varphi-\beta)}\right)\left(2l_c\tan\beta - \frac{f\cos\beta}{2\sin(\varphi-\beta)}\right) \Big/ 2 \tag{10}$$

Once the unequal cutting areas are developed, the skidding cutting force can be calculated based on the mechanistic models of Sui et al. [24] and Lee et al. [25]. The maximum F_{ski} increase with drill skidding can be calculated using Eqs. (6) and (10). It can be found that the unequal cutting areas increase with w, θ, and φ. Specifically, a sharp design with small chisel edge can be a desirable solution to reduce the F_{ski} and subsequently prevent drill skidding during orthopaedic bone drilling. Thus, a cone design is preferred for the first stage of the drill bit to minimize the effect of the chisel edge raising the F_{ski}. Web thinning is applied to the cone tip to create the secondary cutting lips, which can significantly reduce the cutting force and in turn decrease the F_{ski} [29]. However, the length (l) and point angle (δ) of the cone tip would directly affect the maximum inclination angle in surgery according to the geometric relationship. A small δ and large l would not only increase the risk of fracture and the wear of the drill bit, but also increase the difficulty of processing the drill bit and drilling time in surgery. Thus, the optimal δ and l were specified based on experimental testing and the requirements of inclination angle (>45°) in the surgery.

2.2. Thermal and mechanistic analysis

According to the thermal and mechanistic analysis of bone drilling by Sui et al. [24,30] and Lee et al. [25,31], the cutting lips are the main sources of heat and torque, while the chisel edge contributes half of the thrust force under a wide range of drilling conditions. In addition, based on the temperature prediction model established by Feldmann et al. [7,32], the drilling heat can be expressed as a function of the drilling torque as

$$\dot{Q}(t) = M_z(t)\cdot\omega\cdot\left(\frac{M_z(t)}{M_0}\right)^{b-1} \tag{11}$$

where M_0 and b are dimensionless constants which describe the fraction of mechanical energy that is converted to heat and transferred into the bone, and $M_z(t)$ is the axial torque. Specifically, the drill torque could be directly used to evaluate the increase in temperature during bone drilling.

A genetic algorithm-based model for minimizing the thrust force, torque, and temperature was previously developed and experimentally evaluated by the group of authors [33,34], as follows:

Table 1
Comparison of computational optimal thrust force and torque among different calculation weights (1500 rpm, 0.08 mm/rev).

Objectives	Thrust force (N)	Torque (Nmm)
Min $J = F_{th}$ obj1 (Fz))	22.88	60.17
Min $J = 0.75F_{th} + 0.25M_z$ obj2 (Fz&Mz))	23.02	58.35
Min $J = 0.5F_{th} + 0.5M_z$ obj3 (Fz&Mz))	23.23	56.40
Min $J = 0.25F_{th} + 0.75M_z$ obj4 (Fz&Mz))	27.13	55.07
Min $J = M_z$ obj5 (Mz))	30.64	54.55
Control	38.25	65.05

$$\begin{aligned} &Minimize && J = \varsigma_1 F_{th} + \varsigma_2 M_z \\ &&& 45^\circ < \varphi < 75^\circ \\ &s.t. && 0^\circ < \sigma_0 < 36^\circ \\ &&& 17\% < 2w < 25\% \end{aligned} \tag{12}$$

where J is the objective function to be minimised, ς_1 and ς_2 are the calculation weights, and $\varsigma_1 + \varsigma_2 = 1$. F_{th} and M_z are the maximum thrust force and torque during drilling, respectively, which were calculated using mechanistic force model for cutting lips proposed by Sui et al. [24]. The optimised drill bit experimentally presented a significant reduction of the thrust force, torque, and temperature [34]. In optimization, it was found the torque slightly decreases with the increase in ς_2, while the thrust force sharply increases with the decrease in ς_1, as shown in Table 1. Thus, both ς_1 and ς_2 were set as 0.5 for balancing the reduction of maximum thrust force and temperature. The optimal parameters (φ= 45°, σ_0 = 36°, $2w$ = 17%) were used in the current design for reducing the cutting force and temperature increase during bone drilling.

2.3. Mechanical damage

The material failure mechanisms of bones are different from those of metals as they are quasi-brittle and anisotropic. A transition from 'shear' cutting (d_{cut} <10 μm), 'shear crack' cutting (10 μm < d_{cut} <80 μm), and 'fracture' cutting (d_{cut} > 80 μm) models is found with an increase in the uncut chip thickness in orthogonal cutting [18,35], as displayed in Fig. 3 (a–c). The surface roughness is also significantly affected by the changes in the cutting model. A much smaller surface roughness is found under the 'shear' cutting mode than that under the 'fracture & shear crack' cutting conditions. In addition, the required energy is significantly reduced by switching the cutting condition from shear cutting (10 μm < d_{cut}) to fracture cutting (d_{cut} > 90 μm), whereas the instantaneous temperature elevation can be increased with the cutting depth [19]. Specifically, a large d_{cut} could significantly reduce the average temperature elevation during the entire drilling process, whereas a small d_{cut} could reduce the instantaneous temperature without considering the energy accumulation. Therefore, it is desirable that the cutting conditions in the step design changes from 'fracture & shear crack' cutting conditions to 'shear' mode cutting along with drilling for reducing the temperature elevation and improving the surface quality. A transition arc design was proposed as the third step of the drill bit to adjust d_{cut} during the finishing of the drilling, as presented in Fig. 3 (d).

d_{cut} during drilling can be calculated as

$$d_{cut} = \frac{f \sin\alpha}{2} \tag{13}$$

where f is the feeding speed in mm/rev and α is the tangent slope angle at the cutting lips. The cutting depth can be changed by changing α. The arc lip design can smoothly alter the point angle to the desired cutting depth.

The arc centre can be calculated based on the geometrical relationship as

$$(a,\ b) = \left(R - r, \frac{r - r\cos\varphi + R\cos\varphi}{\sin\varphi}\right) \tag{14}$$

where r is the radius of the arc lip and φ is the point angle. Thus, the tangent slope at any point (x_0, z_0) of the arc lips can be calculated as

$$k = \tan\alpha = \frac{x_0 - a}{z_0 - b} \tag{15}$$

The point angle at the arc lip is

$$\alpha_{arc} = \arctan\left(\frac{(x_0 - R + r)\sin\varphi}{z_0 \sin\varphi - r - r\cos\varphi + R\cos\varphi}\right) \tag{16}$$

where (x_0, y_0) follow the relationship as:

$$(x_0 - a)^2 + (z_0 - b)^2 = r^2 \tag{17}$$

The instant point angle of the drill bit with the transition arc design at different cutting depths can be expressed as

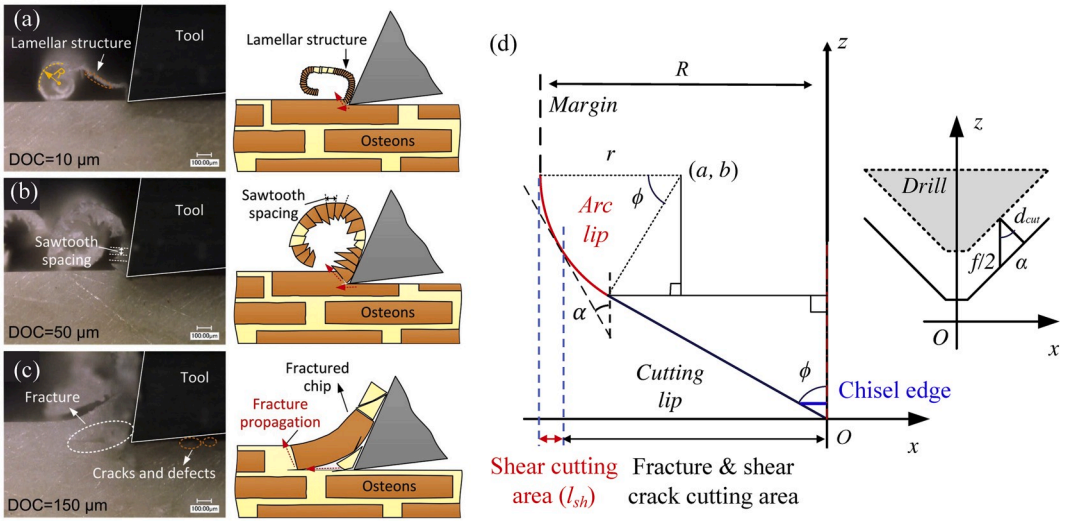

Fig. 3. Chip formation in various DOCs (a–c) [35] and the proposed design concept for the third step of the drill bit (d). ((a, b) is the centre position of arc lip, α is the tangent slope angle at cutting lips, φ is the point angle, f is the feeding speed, d_{cut} is the instantaneous cutting depth).

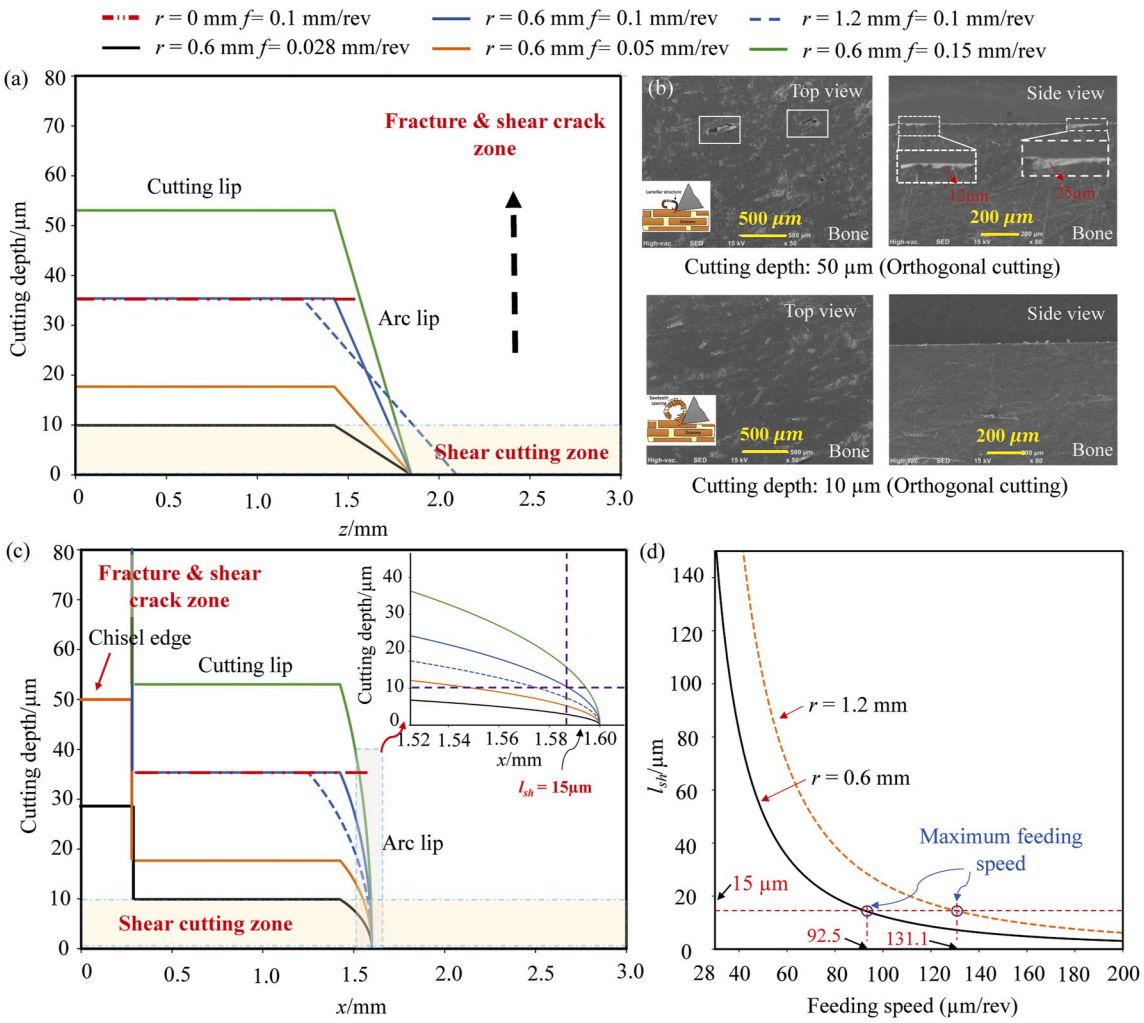

Fig. 4. (a) Variation in cutting depth and cutting mechanism with the tool feed position under different arc radii (r) and feeding speed (f), (b) Variation of surface quality with cutting depth in orthogonal cutting, (c) Variation of the cutting depth with radii of drill bit (x), (d) Relationship between shear cutting area (l_{sh}) with feeding speed. ($\varphi = 45°$).

$$\alpha = \begin{cases} \varnothing & 0 < z < R\cot(\varphi) - r\cot(\varphi) + r\cos(\varphi)\cot(\varphi) \\ \alpha_{arc} & R\cot\left(\varphi\right) - r\cot\left(\varphi\right) + r\cos\left(\varphi\right)\cot\left(\varphi\right) \le z < \dfrac{r - r\cos\varphi + R\cos\varphi}{\sin\varphi} \end{cases} \tag{18}$$

The variation of d_{cut} with the tool feed position (z) under different values of r and f are depicted in Fig. 4 (a). It is confirmed that the cutting model can be switched from the 'shear crack' to the 'shear cutting' cutting condition by the proposed transition arc design with various f. This will not only allow the drill bit to operate with high cutting efficiency and low average temperature elevation, but also decrease the mechanical damage (Fig. 4 (b)) and instantaneous temperature. However, the cutting condition will remains as 'shear cutting' as the f is smaller than 0.028 mm/rev. In addition, it is known that defects can be found as the cutting works on 'fracture' and 'shear crack' cutting conditions in orthogonal cutting, which are around 50 μm and 15 μm respectively [18,35]. Since the f in orthopaedic drilling practically ranges from 0.02 mm/rev to 0.15 mm/rev [3], the cutting model mainly works according to the 'shear crack' cutting condition. Thus, the radial length of drill bit working on the 'shear cutting' model (l_{sh}) (Fig. 3 (d)) should be at least larger than 15 μm in practice so that the recovery of hole quality can be fully realized. Fig. 4 (c) illustrated the variation of the d_{cut} with the radii of drill bit (x). A significant difference in d_{cut} was found among the chisel edge, cutting lips, and arc lips. Fig. 4 (d) illustrates the variation of l_{sh} with the f under different values of r. For the full recovery of hole quality (l_{sh} = 15 μm), the maximum f is 0.093 mm/rev and 0.131 mm/rev when r is set as 0.6 mm and 1.2 mm, respectively. It can be found the l_{sh} decreases with f, while increasing with r. However, it is worthy to note that a large r and small f would increase the cutting time, which would increase the overheat duration in bone drilling.

3. Design and fabrication of low-trauma orthopaedic drill bit

From the above analysis, it can be concluded that a low-trauma orthopaedic drill bit can be proposed based on the step-control scheme approach. Here, each step of the drill bit is designed for specific functions: for preventing drill skidding and reducing the cutting force, temperature, and surface damage. The low-trauma orthopaedic drill bit was designed and patented with three cutting steps, as shown in Fig. 5. The specific functions of each step are as follows.

(1) On entrance, the first step with web thinning of the drill enables centring with a small cutting force when the drill bit is drilled into the bone in the non-perpendicular direction. The specific parameters of the first stage was designed based on the skidding mechanism analysis in section 2.1. The drill skidding can be suppressed by a small F_{ski} and point angle. However, a small point angle will increase the risk of heat accumulation in the first step of drilling.

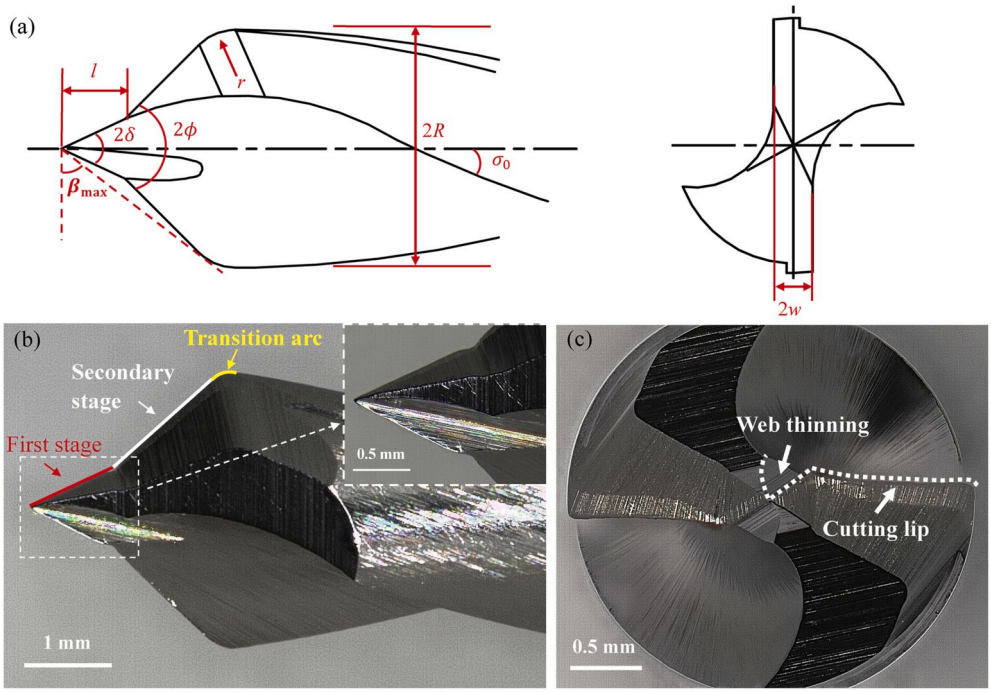

Fig. 5. Geometry design (a) and prototype of the proposed drill bit from the side (b) and bottom (c) views.

(2) The role of the secondary step is to enlarge the hole with an optimal point angle for minimizing the thrust force, torque, and temperature. The area of heat accumulation is rapidly decreased compared to the first step, and a large amount of heat is removed by the chips. The optimised parameters (φ= 45°, σ_0 = 36°, $2w$ = 17%) of the secondary stage was chosen based on the thermal and mechanistic analysis in section 2.2. However, the cutting condition is effective under the 'fracture & shear crack' cutting model during the secondary step of the drilling owing to the large point angle and high feeding speed, which will increase the risk of poor surface quality on the cutting area.

(3) In the third step, the transition arc design is proposed to adjust the point angle during the end of drilling for switching the cutting mechanism from 'fracture & shear crack' cutting to 'shear' cutting when coupled with a certain range of feeding rates. This can reduce the thermal damage and recover the hole quality of the finished hole surface of the bone. The r is set as 0.6 mm for balancing the decrease in surface damage and overheat duration according to the mechanical damage analysis. The suggested f ranges from 0.028 mm/rev to 0.093 mm/rev for switching the cutting conditions efficiently.

The proposed drill bit was fabricated from stainless steel (JIS SUS420J2) from TOKO Co., Ltd. Based on the above analysis and practical experience, the main parameters of the prototype design were identified as: diameter $2R$ = 3.2 mm, point angle of first step 2δ is about 40°–50° (45°), point angle of secondary step 2φ is approximately 90°–100° (90°), radius of the arc lip r is approximately 0.4–0.8 mm (0.6 mm), helix angle σ_0 is 36°, and web thickness $2w$ is 17%. The parameters in brackets are used in the experimental evaluation. The maximum inclination angle (β_{max}) of the proposed drill bit was designed as 54° to satisfy the requirements of surgical operations.

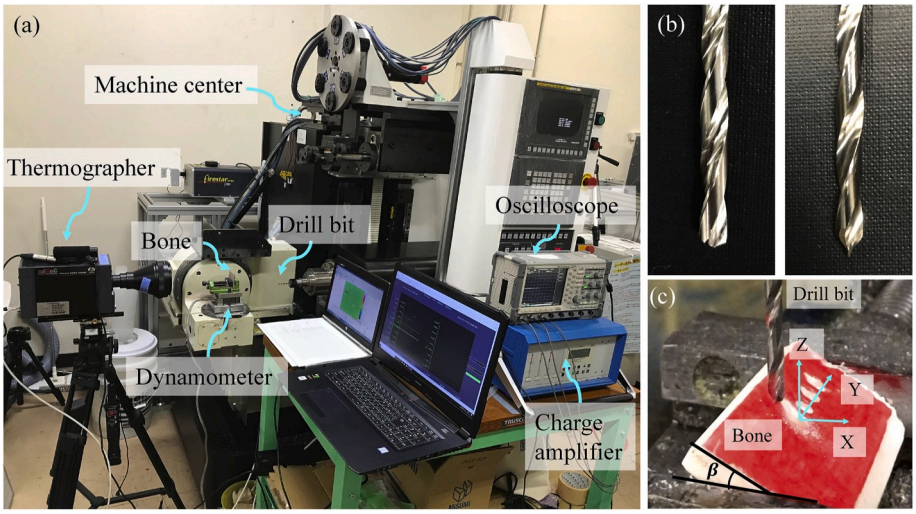

Fig. 6. (a) Experimental setup, (b) Conventional and proposed drill bits used in the experiment, (c) schematics of the drilling in a non-perpendicular direction.

Table 2
Specification of infrared thermal image system.

Resolution	Sampling rate	Spatial resolution	Temperature range
640 pixels × 512 pixels	200 Hz	15 μm/pixel	0 °C–150 °C

4. Experimental verification

4.1. Experimental setup

Evaluation experiments were conducted on a self-developed horizontal five-axis CFRP machining centre with coupled Kistler Dynamometer 9272 and charge amplifier 5070 (sampling frequency: 20 kHz) for the measurement of the cutting forces, as shown in Fig. 6 (a). The performance of the proposed drill bit was evaluated against a conventional drill bit (diameter $2R = 3.2$ mm, point angle 118°, helix angle $\sigma_0 = 36°$, chisel edge angle $\theta = 125°$, and web thickness $2w = 20\%$), as presented in Fig. 6 (b).

It is known that on-site measurement of the temperature characteristics between the bone and drill bit is technically difficult [36]. In addition, the heat is accumulated with the increase of drilling depth and reached the maximum at the bone drill exit. Thus, the thermal characteristics on the drill-exit surface should be considered in bone drilling. In this study, state-of-art microscopy infrared thermography (InfRec H9000 infrared thermography, Nippon Avionics Co., Ltd., Japan), with a high sampling rate (200 Hz) and spatial resolution (15 μm), was performed to record the temperature at the drill-exit plane of the bone. The specifications of the thermography system are listed in Table 2. A calibrated lens extender was used to optically enlarge the focused area and

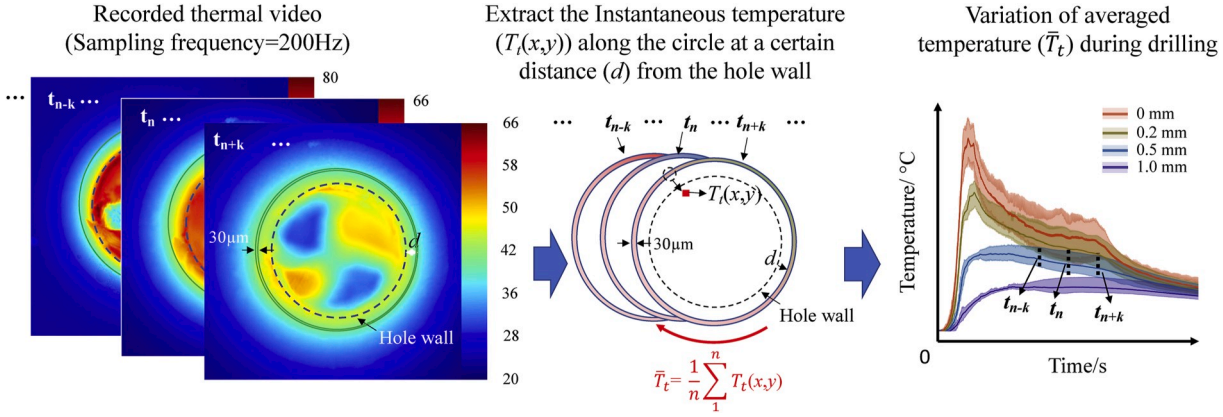

Fig. 7. Data processing workflow of thermal information on the drill-exit surface.

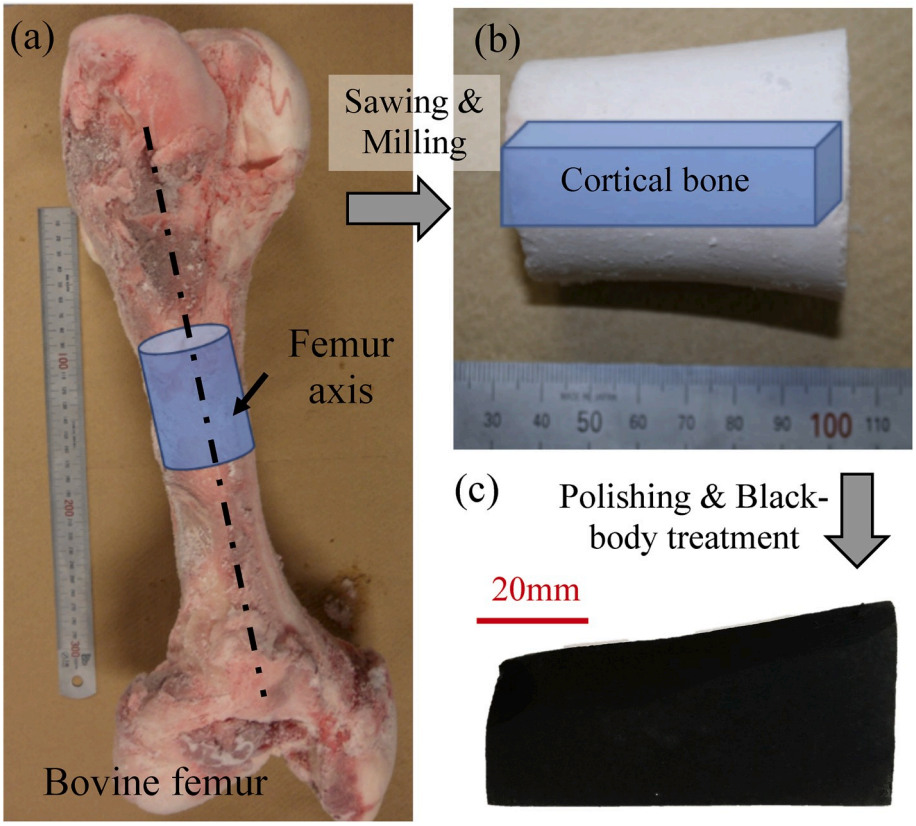

Fig. 8. Preparation of the bone samples.

Table 3
Experimental conditions.

Items	Parameters
Workpiece material	Bovine cortical bone
Thickness (mm)	6
Drill bit diameter (mm)	3.2 mm
Rotation speed (rpm)	1000, 1500, 2000
Feeding speed (mm/rev)	0.05, 0.1
Slope angle (°)	0, 15, 30, 45
Feeding depth (mm)	15
Experimental temperature (°C)	23

Table 4
Comparison of averaged maximum temperature and overheating ($T_{bone} \geq 47$ °C) duration at 0.25 mm from the hole wall.

Drill type	Feeding speed (mm/rev)	Rotation speed (rpm)	Maximum temperature (°C)	Overheating duration (s)
Conventional drill	0.05	1000	58.9 (±2.9)	5.1 (±0.6)
		1500	61.3 (±2.5)	5.6 (±0.4)
		2000	64.1 (±2.3)	6.2 (±0.3)
	0.1	1000	55.4 (±3.2)	4.1 (±0.3)
		1500	58.4 (±2.6)	4.9 (±0.3)
		2000	59.5 (±2.8)	6.1 (±0.5)
Proposed drill	0.05	1000	51.6 (±2.7)	3.4 (±0.2)
		1500	52.3 (±2.6)	3.5 (±0.4)
		2000	55.1 (±3.2)	3.4 (±0.3)
	0.1	1000	47.5 (±3.2)	2.5 (±0.2)
		1500	49.3 (±1.2)	2.9 (±0.5)
		2000	49.6 (±2.6)	3.3 (±0.5)

enable microscale analysis. Black-body treatment can efficiently increase the accuracy of temperature measurement [37]. Thus, a black-body spray (Tasco Co. ltd, Japan) was applied on the samples, and the emissivity was set as 0.94. Thus, the temperature characteristics at the drill-exit plane were used to evaluate the ability of thermal control of the proposed drill bit during dynamic drilling. However, the temperature distribution of the drill bit could not be accurately measured owing to the strong reflections at its smooth surfaces. Therefore, this study mainly focuses on the temperature at the drill-exit plane of the bone, and the recorded data were postprocessed for further analyses. The detailed data processing workflow of thermal information on drill-exit surface is shown in Fig. 7. The confidence interval was set as 95% to remove the effect of random error on the results. The width of the extracted circle, which was used for calculating the specific temperature on a certain distance from the hole wall, was set as the width of 2 pixels (30 μm) to increase the credibility of temperature results. In addition, irrigation was not conducted during the drilling experiment for better observation, although this is the case for controlling the temperature increase of the bone in some orthopaedic surgeries.

4.2. Preparation of bone specimens

The fresh femur of a bovine (age 3–4 years) was used as the workpiece during the experimental verification because its material properties are like those of human cortical bone. The cortical bone specimens were prepared along the axial direction of the femur, as shown in Fig. 8. The prepared samples were cut into 60 mm (length) × 30 mm (width) × 6 mm (thickness) pieces and polished with 400-grit to 1200-grit sandpapers; they were kept in a saline solution and stored in −70 °C and thawed in a saline solution before experiments. The bone sample was cut into 6 mm pieces because most of the cortical bone of humans is thinner than 6 mm [38]. It should be noted that the thickness of the specimens was accurately controlled (error = ±0.05 mm) for removing the potential effect of bone thickness on the temperature increase. In total, ten cortical bone specimens were used in the experiments.

4.3. Experimental procedure

The experimental procedure was designed to evaluate the drilling performance of the proposed drill bit in terms of the drill cutting force, temperature increase, drill skidding, surface quality, and wear with the control of the conventional drill bit. The thrust force and temperature increase were measured simultaneously by the developed experimental setup during drilling of the cortical bone sample in the perpendicular direction. The rotation speed and feeding speed have influence the drilling performance considerably. Thus, six experiments that consider parameters widely used in orthopaedic surgeries were conducted, which are summarised in Table 3. Moreover, delamination and microcracking around the hole surface were observed via laser scanning confocal microscopy (LSCM, Olympus, OLS4100, Japan). For the evaluation of the drill skidding in the proposed design, the bone samples were inclined at specific slope angles ($\beta = 0°$, 15°, 30°, and 45°). The surface was printed in red for better video recording of the drill skidding, as shown in Fig. 6 (c). The skidding forces in the X and Y directions were measured during non-perpendicular drilling and were used to evaluate the self-centring ability of the drill. In addition, the topography of the hole at the entrance surface were measured via optical surface microscopy (Keyence, VR-3000, Japan).

All the experiments were performed five times under each experimental condition. The statistical analysis of the average peak thrust forces and temperature was conducted using the analysis of variance (ANOVA) with the control of the conventional drill bit.

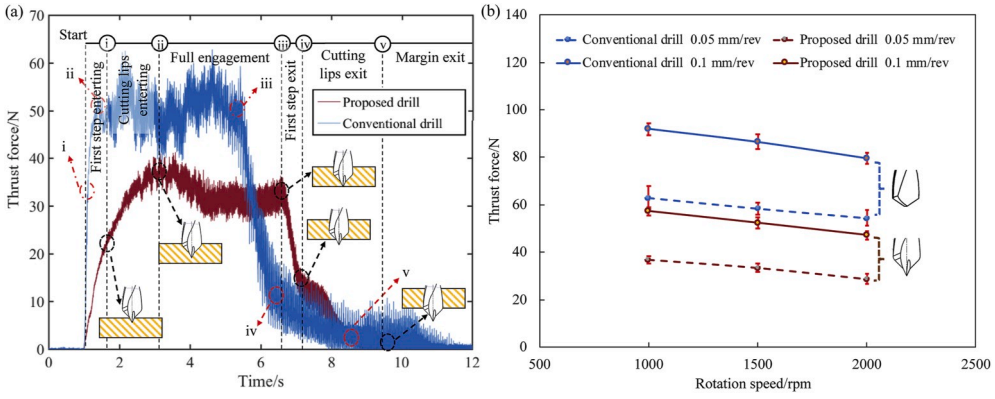

Fig. 9. Comparison of thrust forces of the proposed and conventional drill bits. (a) Thrust forces of the two drill bits (1000 rpm, 0.05 mm/rev), (b) Maxi–means of the thrust forces.

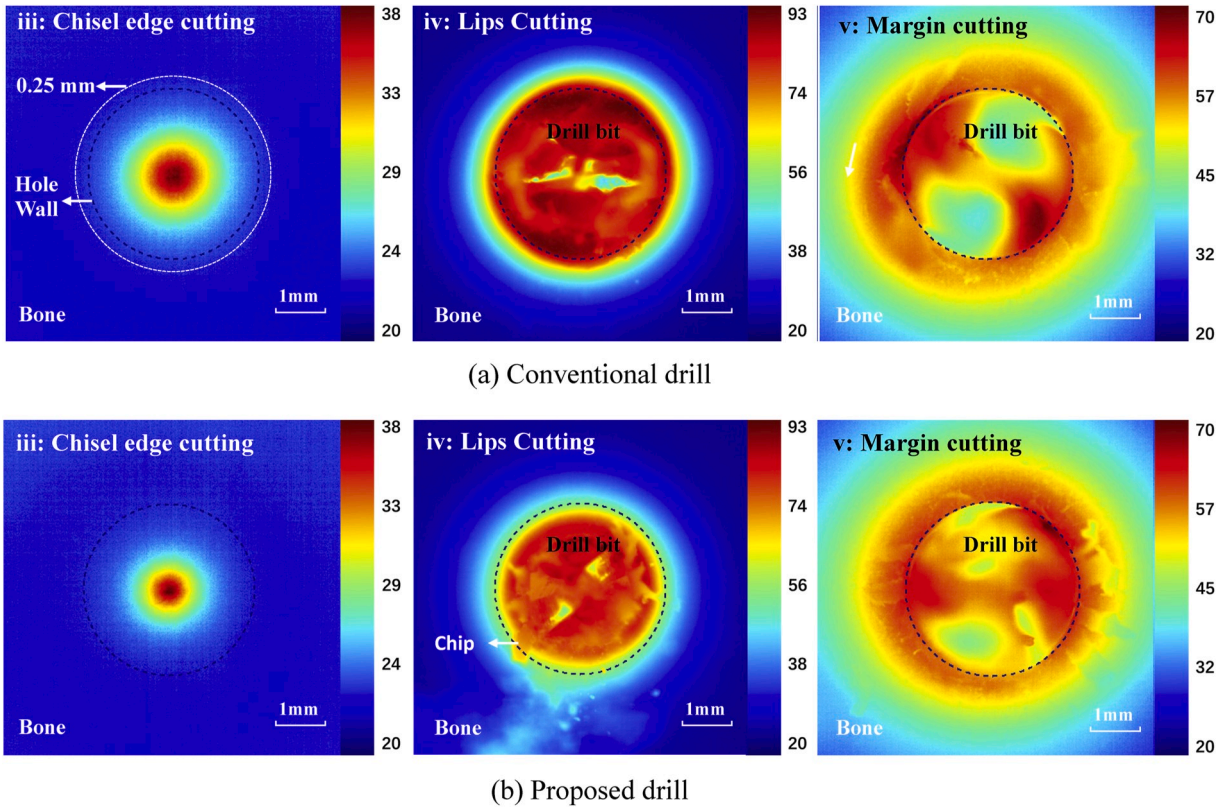

Fig. 10. Comparison of drill-exit temperature distributions of the conventional (a) and proposed (b) drill bit. (1000 rpm, 0.05 mm/rev).

5. Results and discussion

The novel self-centring drill bit design has been proposed based on the theoretical analysis of drill skidding and thermal, mechanistic and material removal mechanisms. Comprehensive experiments were implemented to evaluate the drilling performance of the proposed drill bit in terms of drill cutting force, temperature rise, drill skidding, surface quality, and wear with the control of conventional drill bit.

5.1. Cutting force

A basic step in evaluating the performance of a surgical drill bit is the investigation of the cutting force. The curves of the typical thrust forces of the conventional and proposed drill bits are depicted in Fig. 9 (a) (rotation speed: 1000 rpm, feeding speed: 0.05 mm/rev). A much smaller thrust force is measured on the proposed drill bit ($F_{max} = 37.8$ N) when compared to that on the conventional drill bit ($F_{max} = 55.4$ N). A smoother force pattern is also observed on the proposed drill bit compared to that on the conventional drill bit during the period of full engagement of drilling. This can provide better tactile feedback during surgery and in turn, reduce the fatigue of the surgeon.

For a better understanding of the mechanistic characteristics during drilling, five drilling stages were divided based on the characteristics of the thrust force and the relative positions of the drill bit and bone specimens, which are illustrated in Fig. 9(a). At the first step, the thrust force increases sharply as the chisel edge of the conventional drill bit and the first step of the proposed drill bit penetrate the bone surface. Subsequently, it increases the relative area in the stage where it enters the cutting lips until the cutting lips are involved in the drilling. At full engagement, the cutting lips and chisel edge penetrate the bone. In this period, the thrust force is stabilised for some time, and the small variation may be attributed to the 'fracture and shear crack' cutting model of the bone drilling. The first stage is deemed complete when the first step of the drill penetrates the exit-plane of the bone surface, and the thrust force is significantly decreased. It can be found that the first step of the proposed drill bit increases approximately 52.3% (21.4 N) of the total thrust force, which is approximately 63.5% (33.6 N) for the conventional drill. The stage of the cutting lips and the margin exit is the end of the drilling period of the cutting lips and the entire finishing period of the transition arc cutting lips. A relatively longer drilling time is found with the proposed drill bit (9.8 s) than that with the conventional drill bit (8.5 s) owing to the longer drill tips. In addition, Zhang et al. [27], proposed that a low force could not result in a significantly low damage on the hole in bone drilling. Thus, an in-vivo histological comparison between conventional and proposed drill bit should be considered in the future work.

The maximum thrust force was calculated from the filtered thrust force data, which were filtered by a sixth-order low-pass Butterworth filter having 100 Hz cut-off frequency. Fig. 9(b) shows the effects of the feeding speed and rotation speed on the maximum thrust force during bone drilling by the proposed and conventional drill bits. It can be concluded that the proposed drill bit significantly reduces the thrust force relative to the conventional drill bit under the current experimental conditions. The significant reduction in the thrust force can be explained by the optimised point angle of the secondary cutting edge and the web thinning design of the proposed drill bit. However, Sui et al. (2018) [34] presented a relatively better reduction rate (57.7%) than that in this study (45%). It is mainly caused by the difference in the performance of the control group. The maximum thrust force is approximately 68.8 N (1500 rpm, 0.032 mm/rev) in their control group, while a relatively smaller thrust force (39.2 ± 2.8 N) under the same process condition was found in this study.

5.2. Cutting temperature

Fig. 10 displays the typical temperature distributions during chisel edge cutting (Point iii), lip cutting (Point iv), and margin cutting (Point v) of the conventional and proposed drill bits. A remarkable difference

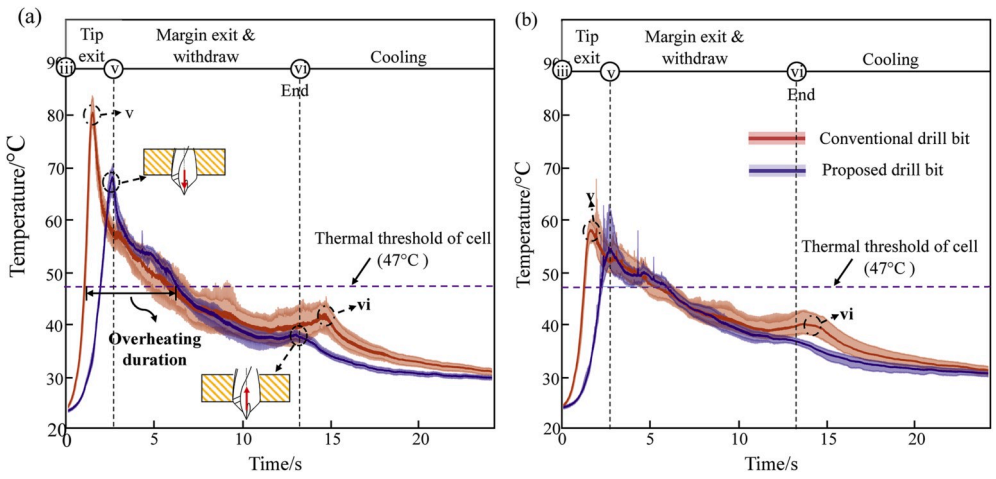

Fig. 11. Temperature variations at the hole wall (a) and 0.25 mm from the hole wall (b) during the bone drilling with the two drill bits. (1000 rpm, 0.05 mm/rev).

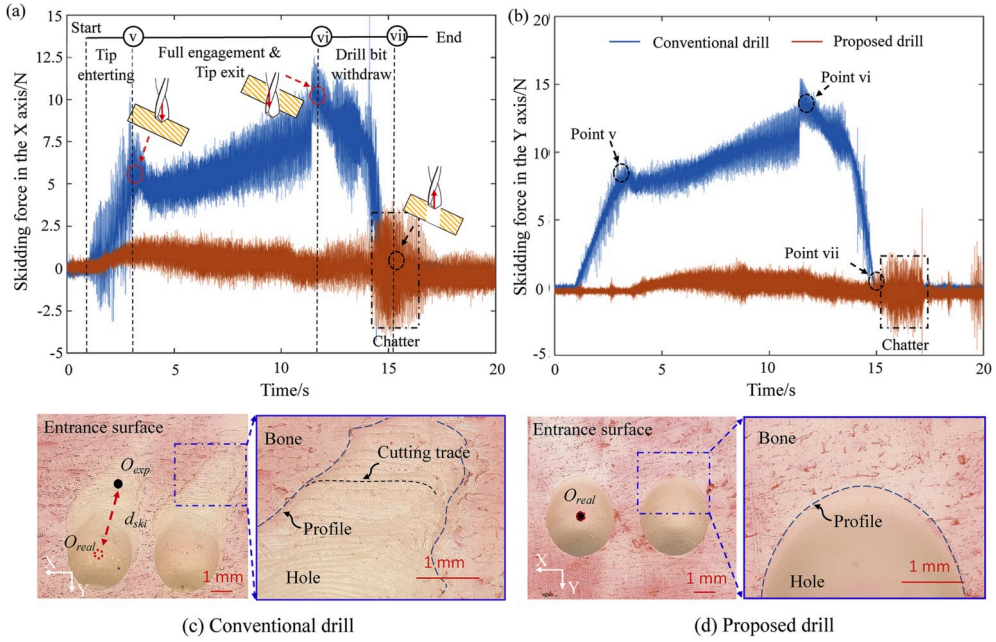

Fig. 12. Comparison of the drill skidding forces in the X (a) and Y (b) axis and the topography image on the entrance surface (c, d) of the conventional and proposed drill bits in non-perpendicular drilling. ($\beta = 30°$, 1000 rpm, 0.05 mm/rev, O_{exp} and O_{real} are the expected and the real hole centres, respectively, d_{ski} is the skidding distance.)

can be found between the two drill bits in the three cutting stages. It is known that the immediate cell damage during bone drilling is dependent not only on the magnitude of the thermal exposure but also on the duration [8]. Thus, the temperature variation at a certain distance from the hole wall were calculated based on the recorded thermal data. The temperature data were initially integrated along the circumference and then averaged, which was considered to be the instantaneous averaged temperature of the focused location. The temperature variations at two locations (0 mm and 0.25 mm) from the hole wall in the drilling with the conventional and proposed drill bits were selected and shown in Fig. 11. The deviation along the focused circle is treated as an envelope in the figure. The average maximum temperature along the hole wall during drilling with a conventional drill (79.8 °C) is much higher than that with the proposed drill bit (68.3 °C), which can also be found at 0.25 mm from the hole wall. In addition, a relatively shorter overheating duration can be found with the proposed drill bit than that with the conventional drill bit. However, a higher peak is observed on the envelope of the proposed drill bit at the tip exit compared with the conventional drill bit, which might be caused by the effect of the cutting chips. The averaged maximum temperature of the proposed design is still higher than the thermal threshold of the cell (47 °C). An internal cooling approach would be an efficient approach to suppress the temperature elevation [14].

Table 4 summarises the average maximum temperature increase and overheating time (T ≥ 47 °C) of the conventional and proposed drill bits at 0.25 mm from the hole wall under different drilling conditions. The proposed drill bit has a superior thermal characteristic, which can reduce the risk of thermal necrosis during bone drilling. Table 4 also illustrates that a high feeding speed with a low rotation speed can efficiently reduce the risk of thermal osteonecrosis of bones. It is also noteworthy, that this is the first-time real-time temperature profiles and temperature variations with high visualisation during bone drilling are presented.

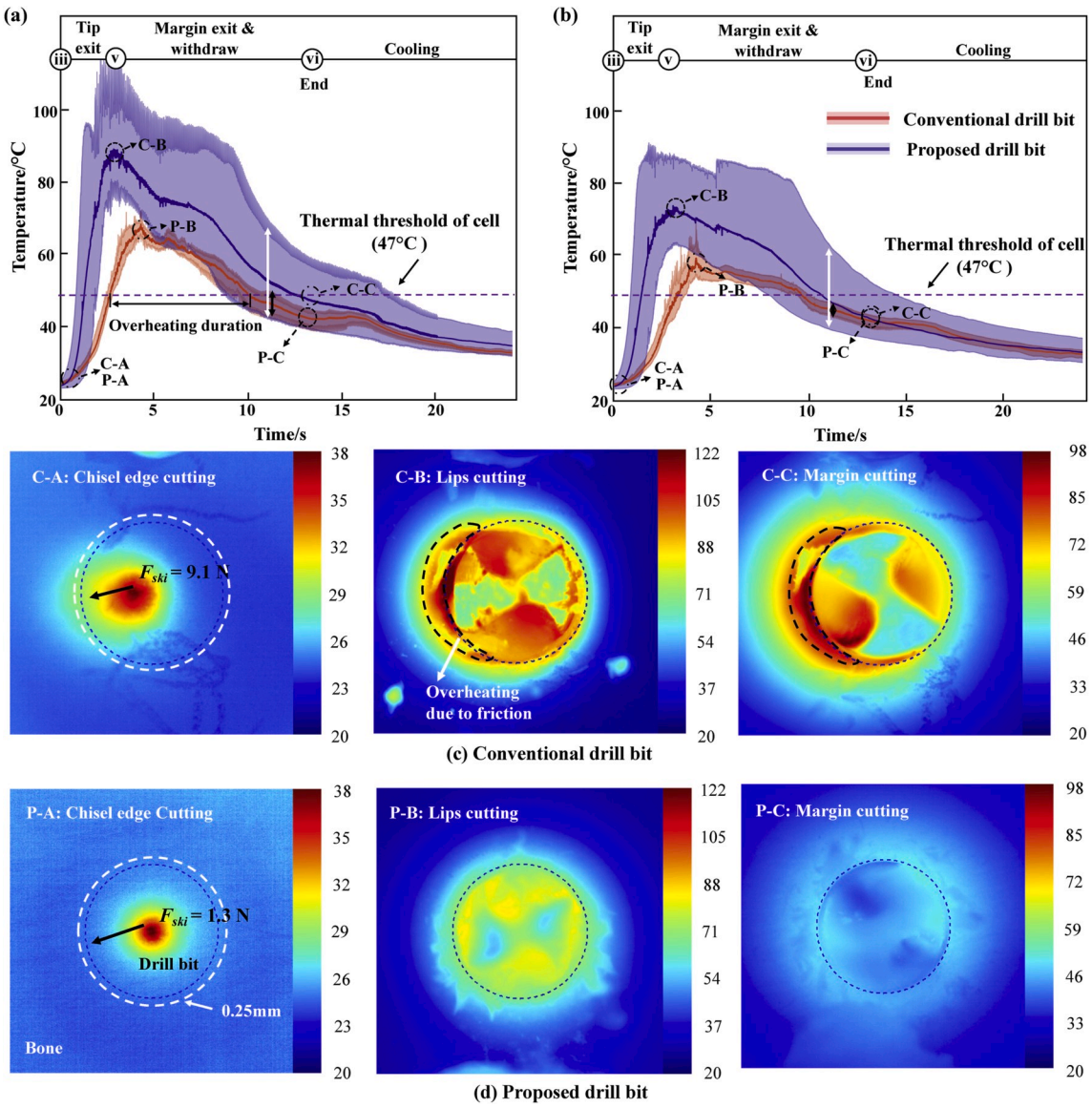

Fig. 13. Comparison at the hole wall (a) and 0.25 mm from the hole wall (b) during the bone drilling with the two drill bits and the drill-exit temperature distributions of the conventional (c) and proposed (d) drill bit. ($\beta = 15°$, 1000 rpm, 0.05 mm/rev).

5.3. Self-centring

The skidding forces in the X axis ($F_{ski\text{-}X}$) and Y axis ($F_{ski\text{-}X}$) during non-perpendicular drilling were used to evaluate the self-centring performances of the drill bits. Much smaller $F_{ski\text{-}X}$ and $F_{ski\text{-}Y}$ are found with the proposed drill bit than with the conventional force during non-perpendicular drilling ($\beta = 30°$), as presented in Fig. 12 (a, b). The drilling can be divided into three stages according to the characteristic of F_{ski}. F_{ski} increases sharply at the initial stage until the drill tip fully penetrates the bone specimen (Point v), and then increases relatively sharply until the feeding of the drill bit reaches the feeding depth (Pint vi). F_{ski} at Point v and Point vi contribute mainly to the bending of the drill bit with the increase in the feed. Maximum F_{ski} can be found at the end of the feeding in non-perpendicular drilling. In addition, it is noteworthy that a noisy force is generated around Point vii, which may increase with the chatter when the drill bit exits the drilled hole. The shorter duration of the stage of drill bit withdrawal is caused by the withdrawal speed being thrice the feeding speed for saving the experimental operation time. Fig. 12 (c, d) presents the topography image of the entrance surface of the hole obtained by the conventional and proposed drill bits. A long skidding distance (d_{ski}) and an irregular hole profile are determined for the hole from the conventional drill bit (Fig. 12(c)), whereas this is rarely observed for the hole drilled by the proposed drill bit (Fig. 12(d)). In Fig. 12(c), there are noticeable cutting traces at the enlarged zone, which are caused by F_{ski} in the non-perpendicular drilling.

In addition, a heat concentration zone was found on the conventional drill bit in non-perpendicular drilling, while it was rarely found on the proposed drill bit, which was explained by the large friction heat between the margin and hole due to the large skidding force, as shown in Fig. 13. The averaged maximum temperature along the hole wall in the drilling with the conventional drill (89.3 °C) is much higher than that with the proposed drill bit (67.4 °C). The overheating duration was also significantly smaller in the proposed design (6.8 s) than that in the conventional drill bit (10.7 s). In other words, the self-centring design could significantly reduce the risk of thermal osteonecrosis of bones during non-perpendicular drilling.

For better evaluation of the self-centring performance of the proposed drill bit at different values of β, the maximum F_{ski} was calculated from the filtered F_{ski} data, which were filtered by a sixth-order low-pass

Table 5
Comparison of maximum skidding force (1000 rpm, 0.05 mm/rev).

Drill type	Slope angle (°)	Maximum $F_{ski\text{-}X}$ (N)	Maximum $F_{ski\text{-}Y}$ (N)
Conventional drill	0	0.8 (±0.2)	0.4 (±0.1)
	15	6.2 (±1.6)	6.7 (±2.4)
	30	10.3 (±1.2))	14.5 (±2.2)
	45	–	–
Proposed drill	0	0.2 (0)	0.2 (0)
	15	1.3 (±0.1)	0.9 (±0.1)
	30	1.7 (±0.1)	1.3 (±0.3)
	45	1.8 (±0.2)	1.7 (±0.4)

Butterworth filter with a 100 Hz cut-off frequency, as summarised in Table 5. Therefore, it can be concluded that the proposed drill bit exhibits a significantly higher self-centring performance than the conventional drill bit, which is the advantage gained from the novel design of the first step of the drill bit.

5.4. Hole quality

Microcracking and delamination of the hole have significant effects on the screw pull-out strength. Fig. 14 compares the hole quality achieved by the conventional and proposed drill bits. Defects and microcracks can be found around the hole entry surface and hole wall drilled by the conventional drill bit, as shown in Fig. 14(a). By contrast, the proposed drill bit generates a smoother surface because of the advantage of the functional transition arc design, as displayed in Fig. 14(b). A damage factor (F_s) was introduced to evaluate the surface quality obtained by the two drill bits, as

$$F_s = D_{\max}/D \tag{19}$$

Where $D_{\max}$ and D are the maximum diameters of a circle enclosing the damaged area and the diameter of the drilled hole, as shown in Fig. 14 (a). The calculated results are provided in Table 6. It can be found that a much better surface quality is achieved by the proposed drill than that by the conventional drill bit. In addition, a worse hole quality is obtained by the conventional drill bit at high feeding speeds and rotation speeds owing to the deep cutting depth.

These disparities are mainly caused by the differences in the cutting mechanisms of the two drill bits. The conventional drill bit can increase the cracks on the surface when working under the 'fracture & shear crack' cutting mode. In comparison, the proposed drill bit performs a finishing action on the surface by adjusting the point angle to switch the cutting model from 'fracture & shear crack' cutting to 'shear' cutting. Therefore, the proposed drill bit significantly reduces the effect of fracture cutting and minimises the surface damage, thereby increasing the screw pull-out strength and benefiting bone regeneration.

5.5. Wear analysis

An orthopaedic drill bit can be used for drilling only once without recycling. However, in practical applications, surgeons are prone to using one drill in an operation with 1–5 holes for reducing the surgery intervention time. Fig. 15 presents the wear performances of the

Table 6
Comparison of the hole damage in two drill bits.

Drill type	Feeding speed (mm/rev)	Rotation speed (rpm)	F_s
Conventional drill	0.05	1000	1.046 (±0.008)
		1500	1.052 (±0.006)
		2000	1.063 (±0.011)
	0.1	1000	1.065 (±0.015)
		1500	1.078 (±0.011)
		2000	1.077 (±0.009)
Proposed drill	0.05	1000	1.002 (±0.001)
		1500	1.002 (±0.001)
		2000	1.000 (±0.001)
	0.1	1000	1.003 (±0.001)
		1500	1.002 (±0.001)
		2000	1.003 (±0.001)

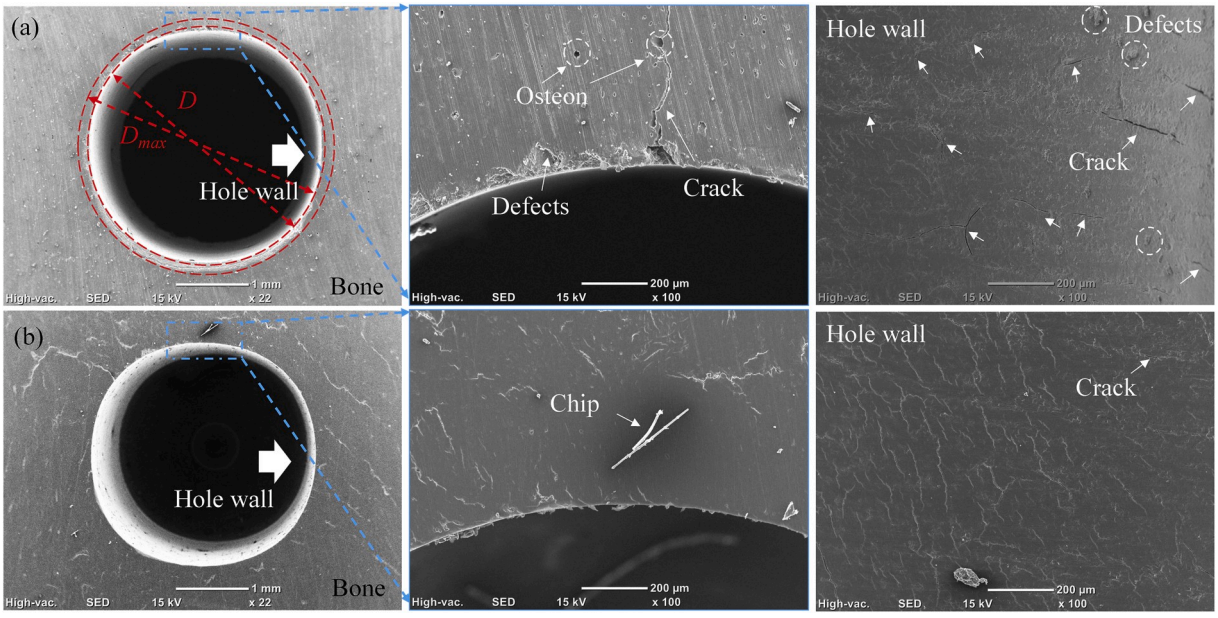

Fig. 14. Comparison of the hole quality obtained by the conventional (a) and proposed (b) drill bits (1000 rpm, 0.05 mm/rev).

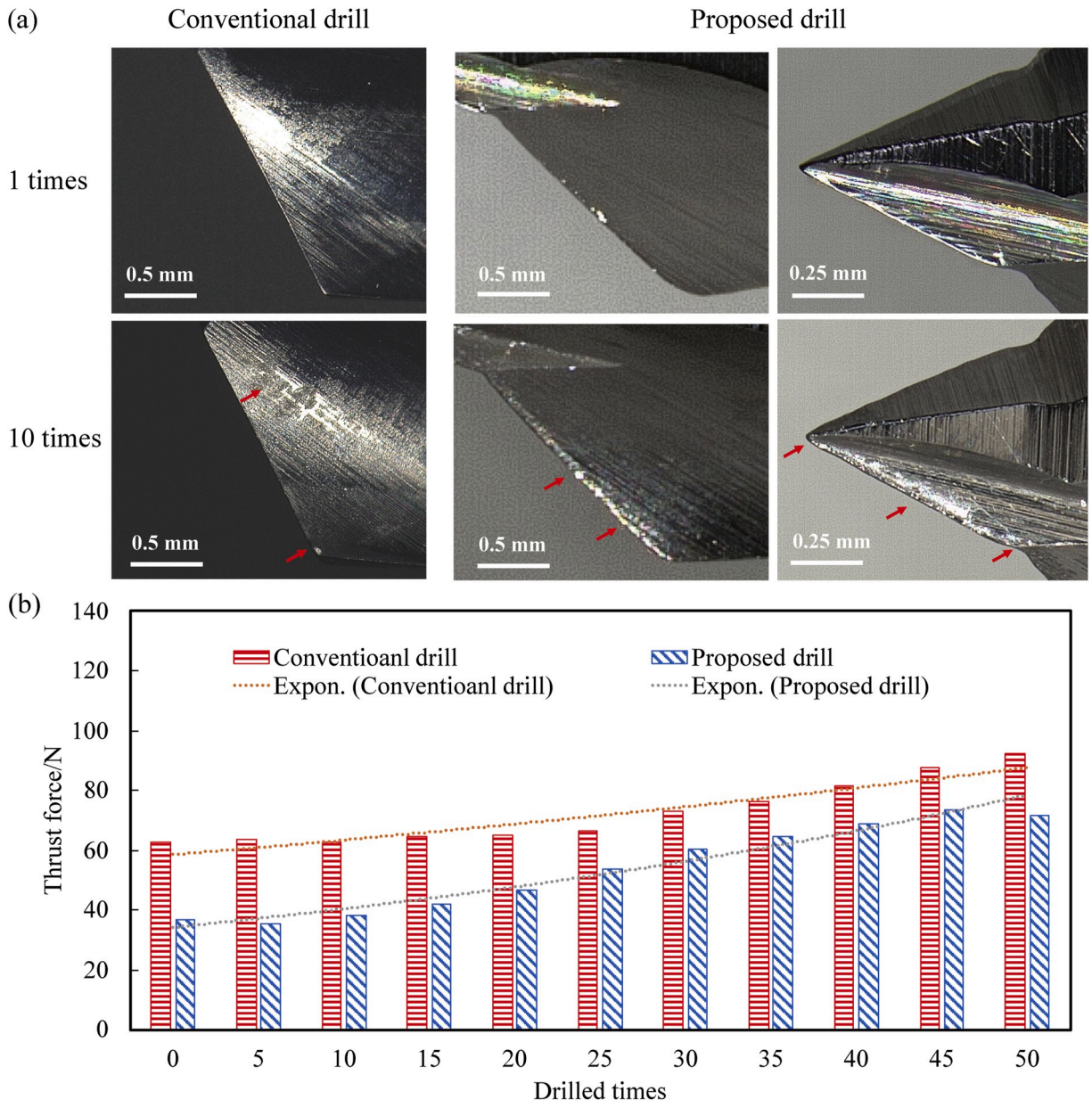

Fig. 15. Wear analysis of the two drill bits. (a) Images of the drill bits after usage, (b) The variation in the thrust force due to the wear with the drilling time. (1000 rpm, 0.05 mm/rev).

conventional and proposed drill bits. A relatively small wear can be found for both the drill bits after one time, whereas considerable wear is observed for the first step of the proposed drill after ten times, as shown in Fig. 15(a). This suggests that the drilling time of the proposed drill should be within ten times, according to the analysis of variation of the thrust force (Fig. 15(b)), to satisfy the requirements of orthopaedic surgeries. In addition, there is no chipping and deformation of the proposed drill bit during the entire experiment. The area of wear and tear on the conventional and proposed drill bits happen mainly on the chisel edge (first step) and grooves, which means that most of the metal particles will be removed with the cutting chips. Thus, a low risk of pollution or inflammation caused by the metal particles could be expected.

6. Conclusions

Drilling is one of the most common and technically demanding procedures in orthopaedic surgery. In this study, a comprehensive theoretical analysis was conducted for examining the main challenges that arise during orthopaedic drilling. A novel drill bit design concept that satisfies the requirements of a low drill force, temperature, and surface damage as well as self-centring was presented based on the analysis of the thermo-mechanistic, drill skidding, and material failure mechanisms of a bone. To evaluate the proposed low-trauma drill bit, comprehensive experiments were conducted. Some of the key conclusions of the study are as follows:

(1) The theoretical analysis of drill skidding indicates that the skidding force increases mainly due to the unequal cutting areas on the chisel edge of the drill. A sharp design with a small chisel edge has the potential to reduce F_{ski} and subsequently suppress drill skidding during orthopaedic bone drilling, which was confirmed by the experimental results. In addition, the self-centring design could significantly reduce the risk of thermal osteonecrosis of bones during non-perpendicular drilling.

(2) The cutting lips are the main source of the heat and thrust force. Thus, the use of an optimal point angle of the cutting lips based on thermo-mechanistic analysis has the capability to balance the effect of the cutting forces and temperature. The experimental results identified that the proposed parameters could significantly reduce the thrust force (more than 45%) and temperature elevation (more than 10%).
(3) The transition arc design could successfully improve the hole quality by switching the cutting mechanism from 'fracture & shear crack' cutting to 'shear' cutting on coupling with a certain range of the feeding rate.
(4) From the drilling experiments, it was found that the proposed drill significantly reduced the drilling force and temperature while improving the position accuracy and surface quality in comparison with the conventional drill design. The proposed drill design provides an effective tool to achieve low-trauma bone drilling in orthopaedic surgery.

Competing interests

None declared.

CRediT authorship contribution statement

Liming Shu: Writing - original draft, Conceptualization, Methodology, Formal analysis, Investigation. **Shihao Li:** Formal analysis, Investigation. **Makoto Terashima:** Methodology, Resources. **Wei Bai:** Data curation. **Takayoshi Hanami:** Writing - review & editing. **Ryo Hasegawa:** Resources. **Naohiko Sugita:** Writing - review & editing, Supervision, Funding acquisition.

Acknowledgments

The authors thank Miss. Koarai Aki and Mr. Matsui Motoomi from Nippon Avionics Co., Ltd for advice and discussion on the temperature during the experiment. The authors would thank the great help from Dr. Zhenlong Fang from the University of Tokyo in the experiments. The authors would also thank the help in the theoretical optimization of the drill bit from Prof. Jianbo Sui from the Guangdong University of Technology.

Appendix A. Supplementary data

Supplementary data to this article can be found online at https://doi.org/10.1016/j.ijmachtools.2020.103568.

Declaration of interests

The authors declare that they have no known competing financial interests or personal relationships that could have appeared to influence the work reported in this paper.

References

[1] W. Bonfield, Advances in the fracture mechanics of cortical bone, J. Biomech. 20 (1987) 1071–1081, https://doi.org/10.1016/0021-9290(87)90025-X.
[2] R.K. Pandey, S.S. Panda, Drilling of bone: a comprehensive review, J. Clin. Orthop. Trauma. 4 (2013) 15–30, https://doi.org/10.1016/j.jcot.2013.01.002.
[3] J.E. Lee, C.L. Chavez, J. Park, Parameters affecting mechanical and thermal responses in bone drilling: a review, J. Biomech. 71 (2018) 4–21, https://doi.org/10.1016/j.jbiomech.2018.02.025.
[4] G. Augustin, T. Zigman, S. Davila, T. Udilljak, T. Staroveski, D. Brezak, S. Babic, Cortical bone drilling and thermal osteonecrosis, Clin. Biomech. 27 (2012) 313–325, https://doi.org/10.1016/j.clinbiomech.2011.10.010.
[5] D. Axinte, Y. Guo, Z. Liao, A.J. Shih, R. M'Saoubi, N. Sugita, Machining of biocompatible materials — recent advances, CIRP Ann 68 (2019) 629–652, https://doi.org/10.1016/j.cirp.2019.05.003.
[6] G.F. Tawy, P.J. Rowe, P.E. Riches, Thermal damage done to bone by burring and sawing with and without irrigation in knee arthroplasty, J. Arthroplasty 31 (2016) 1102–1108, https://doi.org/10.1016/j.arth.2015.11.002.
[7] A. Feldmann, J. Anso, B. Bell, T. Williamson, K. Gavaghan, N. Gerber, H. Rohrbach, S. Weber, P. Zysset, Temperature prediction model for bone drilling based on density distribution and in vivo experiments for minimally invasive robotic cochlear implantation, Ann. Biomed. Eng. 44 (2016) 1576–1586, https://doi.org/10.1007/s10439-015-1450-0.
[8] E.B. Dolan, M.G. Haugh, D. Tallon, C. Casey, L.M. McNamara, Heat-shock-induced cellular responses to temperature elevations occurring during orthopaedic cutting, J. R. Soc. Interface 9 (2012) 3503–3513, https://doi.org/10.1098/rsif.2012.0520.
[9] E. Jantunen, A summary of methods applied to tool condition monitoring in drilling, Int. J. Mach. Tool Manufact. 42 (2002) 997–1010, https://doi.org/10.1016/S0890-6955(02)00040-8.
[10] N. Bertollo, T.K. Gothelf, W.R. Walsh, 3-Fluted orthopaedic drills exhibit superior bending stiffness to their 2-fluted rivals: clinical implications for targeting ability and the incidence of drill-bit failure, Injury 39 (2008) 734–741, https://doi.org/10.1016/j.injury.2007.11.286.
[11] H.T. Lakshmikantha, N.K. Ravichandran, M. Jeon, J. Kim, H.S. Park, 3-Dimensional characterization of cortical bone microdamage following placement of orthodontic microimplants using Optical Coherence Tomography, Sci. Rep. 9 (2019) 1, https://doi.org/10.1038/s41598-019-39670-9.
[12] Z. yuan Jia, C. Zhang, F. ji Wang, R. Fu, C. Chen, An investigation of the effects of step drill geometry on drilling induced delamination and burr of Ti/CFRP stacks, Compos. Struct. 235 (2020) 111786, https://doi.org/10.1016/j.compstruct.2019.111786.
[13] L. Shu, N. Sugita, T. Shimada, K. Yamamoto, T. Kizaki, M. Mitsuishi, Design and experimental analysis of step drills aiming orthopedic surgery, in: 31th Am. Soc. Precis. Eng., 2016.
[14] G. Augustin, S. Davila, T. Udilljak, T. Staroveski, D. Brezak, S. Babic, Temperature changes during cortical bone drilling with a newly designed step drill and internally cooled drill, Int. Orthop. 36 (2012) 1449–1456.
[15] N. Sugita, M. Mitsuishi, Specifications for machining the bovine cortical bone in relation to its microstructure, J. Biomech. 42 (2009) 2826–2829, https://doi.org/10.1016/j.jbiomech.2009.08.017.
[16] N. Sugita, T. Osa, R. Aoki, M. Mitsuishi, A new cutting method for bone based on its crack propagation characteristics, CIRP Ann. - Manuf. Technol. 58 (2009) 113–118, https://doi.org/10.1016/j.cirp.2009.03.057.
[17] H. He, C. Wang, Y. Zhang, Y. Zheng, L. Xu, G. Xie, D. Zhao, B. Chen, H. Chen, Investigating bone chip formation in craniotomy, Proc. Inst. Mech. Eng. Part H J. Eng. Med. 231 (2017) 959–974, https://doi.org/10.1177/0954411917727245.
[18] Z. Liao, D.A. Axinte, On chip formation mechanism in orthogonal cutting of bone, Int. J. Mach. Tool Manufact. 102 (2016) 41–55, https://doi.org/10.1016/j.ijmachtools.2015.12.004.
[19] A. Feldmann, P. Ganser, L. Nolte, P. Zysset, Orthogonal cutting of cortical bone: temperature elevation and fracture toughness, Int. J. Mach. Tool Manufact. (2017) 118–119, https://doi.org/10.1016/j.ijmachtools.2017.03.009, 1–11.
[20] N. Sugita, K. Ishii, J. Sui, M. Terashima, Multi-grooved cutting tool to reduce cutting force and temperature during bone machining, CIRP Ann. - Manuf. Technol. 63 (2014) 101–104, https://doi.org/10.1016/j.cirp.2014.03.069.
[21] Z. Liao, D.A. Axinte, D. Gao, A novel cutting tool design to avoid surface damage in bone machining, Int. J. Mach. Tool Manufact. 116 (2017) 52–59, https://doi.org/10.1016/j.ijmachtools.2017.01.003.
[22] L. Shu, N. Sugita, Analysis of fracture , force , and temperature in orthogonal elliptical vibration-assisted bone cutting, J. Mech. Behav. Biomed. Mater. 103 (2020) 103599, https://doi.org/10.1016/j.jmbbm.2019.103599.
[23] L. Shu, N. Sugita, M. Oshima, M. Mitsuishi, Design and experimental force analysis of a novel elliptical vibration assisted orthopedic oscillating saw, Med. Eng. Phys. 54 (2018) 22–31, https://doi.org/10.1016/j.medengphy.2018.02.005.
[24] J. Sui, N. Sugita, K. Ishii, K. Harada, M. Mitsuishi, Mechanistic modeling of bone-drilling process with experimental validation, J. Mater. Process. Technol. 214 (2014) 1018–1026, https://doi.org/10.1016/j.jmatprotec.2013.11.001.
[25] J. Lee, B.A. Gozen, O.B. Ozdoganlar, Modeling and experimentation of bone drilling forces, J. Biomech. 45 (2012) 1076–1083, https://doi.org/10.1016/j.jbiomech.2011.12.012.
[26] N. Bertollo, H.R.M. Milne, L.P. Ellis, P.C. Stephens, R.M. Gillies, W.R. Walsh, A comparison of the thermal properties of 2- and 3-fluted drills and the effects on bone cell viability and screw pull-out strength in an ovine model, Clin. Biomech. 25 (2010) 613–617, https://doi.org/10.1016/j.clinbiomech.2010.02.007.
[27] Y. Zhang, L. Xu, C. Wang, Z. Chen, S. Han, B. Chen, J. Chen, Mechanical and thermal damage in cortical bone drilling in vivo, Proc. Inst. Mech. Eng. Part H J. Eng. Med. 233 (2019) 621–635, https://doi.org/10.1177/0954411919840194.
[28] A. Feldmann, J. Wandel, P. Zysset, Reducing temperature elevation of robotic bone drilling, Med. Eng. Phys. 38 (2016) 1495–1504, https://doi.org/10.1016/j.medengphy.2016.10.001.
[29] N. Sugita, M. Oshima, K. Kimura, G. Arai, K. Arai, Novel drill bit with characteristic web shape for high efficiency and accuracy, CIRP Ann 67 (2018) 69–72, https://doi.org/10.1016/j.cirp.2018.04.113.
[30] J. Sui, N. Sugita, M. Mitsuishi, Thermal modeling of temperature rise for bone drilling with experimental validation, J. Manuf. Sci. Eng. Trans. ASME. 137 (2015) 1–10, https://doi.org/10.1115/1.4030880.
[31] J. Lee, Y. Rabin, O.B. Ozdoganlar, A new thermal model for bone drilling with applications to orthopaedic surgery, Med. Eng. Phys. 33 (2011) 1234–1244, https://doi.org/10.1016/j.medengphy.2011.05.014.
[32] A. Feldmann, K. Gavaghan, M. Stebinger, T. Williamson, S. Weber, P. Zysset, Real-time prediction of temperature elevation during robotic bone drilling using the

torque signal, Ann. Biomed. Eng. 45 (2017) 2088–2097, https://doi.org/10.1007/s10439-017-1845-1.
[33] J. Sui, Studies on Mechanics of Bone Drilling and Optimization of Drill Bit Geometry, University of Tokyo, 2014.
[34] J. Sui, N. Sugita, Optimization of drill bits for bone drilling procedure, Proc. ASME 2018 Int. Manuf. Sci. Eng. (2018) 1–8.
[35] W. Bai, L. Shu, R. Sun, J. Xu, V.V. Silbershmidt, N. Sugita, Mechanism of material removal in orthogonal cutting of cortical bone, J. Mech. Behav. Biomed. Mater. 104 (2020) 103618, in press.
[36] J. Lee, O.B. Ozdoganlar, Y. Rabin, An experimental investigation on thermal exposure during bone drilling, Med. Eng. Phys. 34 (2012) 1510–1520, https://doi.org/10.1016/j.medengphy.2012.03.002.
[37] A. Feldmann, P. Zysset, Experimental determination of the emissivity of bone, Med. Eng. Phys. 38 (2016) 1136–1138, https://doi.org/10.1016/j.medengphy.2016.06.019.
[38] S.L. Croker, W. Reed, D. Donlon, Comparative cortical bone thickness between the long bones of humans and five common non-human mammal taxa, Forensic Sci. Int. 260 (2016), https://doi.org/10.1016/j.forsciint.2015.12.022, 104.e1-104.e17.

Nomenclature

2φ: Point angle of drill bit
σ_0: Helix angle
$2R$: Diameter of drill bit
$2w$: Web thickness of drill bit
θ: Angle of chisel edge
$\zeta\eta z$: Rotation coordinate system of drill bit
XYZ: Inertial Cartesian coordinate system
d_{cut}: Cutting depth
β: Slope angle of workpiece
β_{max}: Maximum inclination angle of drill bit
F_{ski}: Drill skidding force in non-perpendicular drilling
$F_{ski\text{-}X}$: Drill skidding force in X direction during non-perpendicular drilling
$F_{ski\text{-}Y}$: Drill skidding force in Y direction during non-perpendicular drilling
d_{ski}: Skidding distance during non-perpendicular drilling
ω: Rotation speed in rad/s
t: Cutting time
f: Feeding speed in mm/rev
l_c: Half-length of chisel edge
T: Rotation period of drilling
ΔA_c: Dynamic chip area difference on chisel edge in non-perpendicular drilling
ΔA_l: Dynamic chip area difference on cutting lip in non-perpendicular drilling
ΔA_{c-max}: The maximum difference of chip area on chisel edge in non-perpendicular drilling
ΔA_{l-max}: The maximum difference of chip area on cutting lip in non-perpendicular drilling
M_0, b: Dimensionless constant that describe the fraction of mechanical energy
J: Objective function
ς_1: , ς_2 Calculation weights and $\varsigma_1 + \varsigma_2 = 1$
F_{th}: Thrust fore during drilling
$M_z(t)$: Torque during drilling
α: Tangent slope angle at cutting lips
α_{arc}: Tangent slope angle at arc lip
r: Radius of the arc lip
F_{max}: Maximum thrust fore during drilling
T_{bone}: Temperature elevation of bone
F_s: Damage factor
D_{max}: Diameter of maximum diameter of a circle enclosing the damaged area
D: Diameter of the drilled hole
l_{sh}: Radial length of drill bit working on the 'shear cutting' model
$T_t(x,y)$: Instantaneous temperature at position (x, y)
d: Distance from the hole wall
$\overline{T_t}$: Averaged temperature elevation at t